Progress on lanthanide sesquioxide phase transition

Simon Guené-Girard, Véronique Jubera, Philippe Brevet, Manuel Gaudon

Progress on lanthanide sesquioxide phase transition

Simon Guené-Girard[1], Véronique Jubera[1], Philippe Brevet[2], Manuel Gaudon[1*]

[1] Univ. Bordeaux, CNRS, Bordeaux INP, ICMCB, UMR 5026, F-33600 Pessac, France

[2] Safran Helicopter Engines, F-64511 Bordes, France

* *manuel.gaudon@u-bordeaux.fr*

KEYWORDS. Phase transition ; Lanthanide sesquioxides ; Crystal structures ; Lattice energy ; Surface energy

Abstract

The present work aims to bring an original approach to the understanding of the polymorphic transition of RE_2O_3 from the low-temperature polymorph to the higher-temperature polymorph: from the cubic C to the hexagonal A form or from the monoclinic C to the monoclinic B form, for which the transition temperatures depend intimately on the rare earth element. The view proposed here, focusing on the lanthanide sesquioxide series, from Nd_2O_3 to Dy_2O_3, includes crystallographic and energetic considerations, using both bulk and surface energy calculations. After a complete description of the polymorphic filiations based on A, B and C unit cells described on simplified RE cation stacking schemes, it will be shown that the growth of the crystallite size as a function of temperature explains the existence of such transitions for these sesquioxides.

1. Introduction

In contrast to the crystallization-melting-recrystallization process, crystalline solid-solid transitions occur only in the ionic, covalent or metallic bonded solid state [1]. Solid-solid phase transitions can be arbitrarily divided into two main categories: "*reversible solid-solid phase transitions"*, which are reversible, with mostly the observation of hysteresis between cooling and heating modes, and *"phase change materials"*, which are not reversible, i.e. used for the transformation of a metastable phase (out of the phase diagram) into a stable allotropic form.

Just focusing on inorganic ionic crystals (with inorganic oxides as main category), the solid-solid transitions take place between two different crystalline forms of a unique compound and, from the thermodynamic standpoint, solid-solid phase transitions are associated with their single robust transition temperature: T_0, at which both the crystalline forms coexist in equilibrium [2]. Whether 1st order or 2nd order, or with a displacive or order-disorder mechanism, the reversible solid-solid phase transitions are the most studied ; reversible phase transitions can imply besides the structural transformation some huge changes in terms of magnetic [3], optical [4], transport (ionic, electronic) [5] or catalytic properties [6]. Reversible phase transition can thus be used in smart/active materials, as for example the metal-insulator phase transition of vanadium dioxide, which is accompanied by a radical change of its transparency in the infrared, is extensively studied for smart window applications [7-11]. Nonetheless, “phase changes”, although not reversible change processes, can also be used in some industrial innovations, such as in thermal or pressure sensing systems [12–18]. Phase changes occur because the crystal structure of the nanocrystal is metastable, meaning only stabilized thanks to the surfaces, which are with lower energies than the stable allotropic form. For well-known example, titanium dioxide (titania) made in the nanophase always adopts the anatase structure. At higher temperatures, the material spontaneously transforms into the bulk rutile stable phase [19–23]. The role of grain size in these metastable to stable phase transitions is crucial. Such a mechanism can be illustrated by superimposing the evolution of the total energy (in $J.cm^{-3}$) as a function of the crystallite size (for crystallites here of cubic shape) for two allotropic forms of different lattice energy (E_r) and surface energy (E_S). In a methodology that will be applied latter in the manuscript, the total volume energy was calculated as $E_{tot}/V = (E_r \times V + E_s \times S)/V = E_r \times a^3 + E_s \times 6 \times a^2$, with a the cube edge length. The "red" form (metastable form, low temperature, nanometric crystallites) of lattice energy less stable than the blue form (stable form) but which has at the same time a surface energy less high than the blue form, will have its total energy crossing that of the stable form at the phase change temperature, for a critical crystallite size of, in this example, 9 nm (Fig. 1).

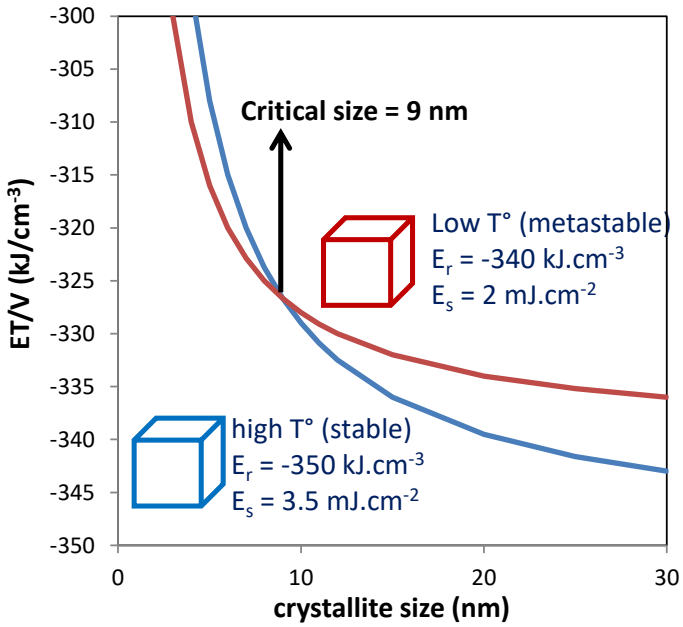

Fig.1 *Evolution of the total energy (Et/V) in kJ.cm^{-3} of two allotropic forms with a phase change*

The polymorphism and thermodynamic properties of lanthanide sesquioxides have been studied since the beginning of the last century [24–30]. Nowadays rare earth (RE) oxides are key materials for electronic, photonic and magnetism, their strategic position justifies the need to better understand their properties. Large differences on the thermodynamic properties of their polymorphic transitions are reported in the literature. Due to strong chemical similarities of the various RE oxides making their metal separation difficult, the oldest studies dating from the beginning of the 19th century suffered from the low purity of the powder available at that time, leading to disparity in the collected data [31]. Three recent reviews gathering thermodynamic properties of rare earth sesquioxide (RE_2O_3) are already published [13, 32–35]. There is now a consensus on a major part of the various RE_2O_3 existing phases, but some differences subsist, about Nd_2O_3 for example. The RE_2O_3 family presents 5 crystallographic forms, first named by Goldschmidt *et al*. [24]: C, B, A, H, X; with C, B and A, three forms which could be stabilized at room pressure, being respectively with cubic, monoclinic and hexagonal crystallographic systems. The temperature range stability of these C, B and A forms are different depending on the RE_2O_3 compound, varying from room temperature and up to 2000 °C. The two last, H and X are respectively hexagonal and cubic high temperatures phases occurring only above 2000°C and/or high pressure, that will not be discussed in the present work. Phase diagram differs

according to the different authors. Based on a critical review of the literature and the present work, we suggest the phase diagram presented in Fig.2. This diagram is consistent with the work of [27,28,34]**.** The room temperature phase for the light rare earth oxide (La to Nd) is only A, except for Nd_2O_3, a stable cubic phase is also found, leading to a C to A transition around 750°C. The middle RE_2O_3 (Pm to Gd) presents two stable forms, C and B, and the heavy RE_2O_3 (Tb to Lu), also presents C and B phase up to Dy_2O_3, for smaller ionic radius only the cubic phase exist.

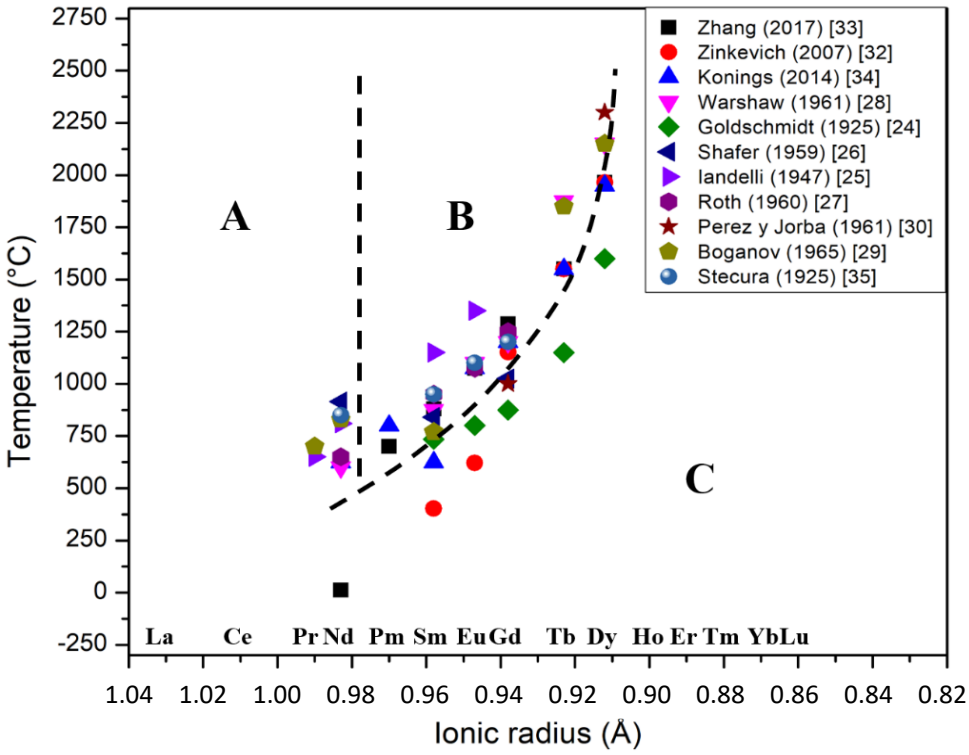

Fig.2 *Literature review on phase-transition temperatures of various lanthanide sesquioxides.*

First it is not always clear from the literature, the cases where the transition temperatures reported are extracted from in-situ characterizations (X-ray diffraction versus temperature) or, in the opposite, from ex-situ techniques after a cooling down to room temperature (with a drastic quenching velocity, or, in the contrary, a very slow cooling-down). Thus, the transition temperatures seem to be subject to a large variability depending on the experimental protocol. This is a key point to apprehend the thermodynamic origin of their solid-state transitions. In respect with the idea that the RE_2O_3 oxides are within the category of reversible solid phase transition materials, Stecura *et al*. [36] have assigned the variability of the reported phase transition temperatures to the importance of the kinetics of the different thermal treatments used depending on the authors. Especially, at this stage, one can enounce

that the lanthanide sesquioxide phase transitions are not clearly classified depending on the two large categories previously discussed, *i.e.* as reversible solid-solid transitions or phase changes. The transitions cited previously are most of the times assumed to be reversible by different authors [26,28,32-35,37], from the high to the low temperature forms which is supposed to have very slow kinetics. As additional argues in favour to the reversible solid-solid phenomenon, Roth and Schneider [27] obtained traces of cubic phase (low temperature form) on the surface of a monoclinic sample of Gd_2O_3, after a 2 weeks thermal treatment at 1200 °C (*i.e.* just below the transition temperature). However, from the appearing crucial role of the grain surfaces, they ambiguously concluded that all the polymorphic transition must be irreversible and monotropic [27]. Shafer and Roy [26] and Warshaw and Roy [28] announced reversibility for various RE_2O_3, but under hydrothermal conditions. Hydrothermal conditions could favour dissolution and re-precipitation of the oxide phases, *i.e.* implying mechanisms out of the scope of the solid phase transitions; thus, the obtaining of low temperature form did not prove the reversibility of the solid-solid phase transition of the Re_2O_3 compounds. Most of the other authors did not bring any evidence of reversibility. Stecura *et al*. [36] heated several RE_2O_3 compounds in their high temperature phase below the transition temperature, and none reversibility effect was observed. Dogmatically, firmly believing that the phase transition of lanthanide sesquioxides must be classified as reversible phase transitions, they explained the as-observed irreversibility by the insufficient thermal energy, while temperature is fixed below the transition temperature, to overcome the ionic interactions that block such a reconstructive transition.

The present work intends to bring a new approach to the understanding of the polymorphic transition of RE_2O_3 from the low temperature polymorph to the higher temperature one: from C to A and from C to B transitions, depending on the RE element. The vision proposed here, focused on the lanthanide sesquioxide series from Nd_2O_3 to Dy_2O_3 includes crystallographic and energetic considerations, using both volume (bulk) and surface energy calculations. After a full new description of the polymorph filiations basing on the A, B and C unit-cells described on simplified RE cation patterns and stacking, the triple correlation between crystallite size evolution (growth), the RE ionic radius and the transition temperature of such Re_2O_3 phase transitions is investigated and disentangled.

2. Experimental section

Neodymium oxide 99.99 % was purchased at Alfa Aesar, samarium oxide 99.9 % was purchased at ampere industry, gadolinium oxide 99.99 % was purchased at Reacton and aluminium oxide (99.99%, sintered at 1700°C) was purchased at Koch-Light Laboratories Ltd.

Pure Nd_2O_3 (neodymium oxide) is usually produced within its hexagonal phase with traces of cubic phase (this is the case for the Alfa Aeser sample). In order to produce pure cubic phase (low temperature form), the commercial Nd_2O_3 powder was first peptized into excess of water to lead to $Nd(OH)_3$ formation. For such step, argon gas flux was continuously bubbled into the aqueous solution for 20 min to avoid the formation of carbonate from dissolve CO_2 (*i.e.* CO_2,H_2O - H_2CO_3) The solution was kept under stirring during 5 days. To obtain pure cubic Nd_2O_3, the dried hydroxide was calcined during 1 hour at 500°C under air. In addition, at the end of the paper, cubic Nd_2O_3 powder was mixed with Al_2O_3 in a mortar to check the impact of Nd_2O_3 crystallite size on the cubic to monoclinic phase change temperature (the 80 wt% alumina in the Al_2O_3/Nd_2O_3 mixture retarding the growth of Nd_2O_3 crystallites compared to the pure Nd_2O_3 sample). Pure cubic Nd_2O_3 and Nd_2O_3 mixed with Al_2O_3 are then thermally treat during 10 min, at temperature from 800°C to 1050°C with step of 50°C.

Alfa Aeser Sm_2O_3 (samarium oxide) and Reacton Gd_2O_3 (gadolinium oxide) raw powder exhibits only the low temperature phase and were used without any additional treatment.

For phase transition reversibility tests, neodymium, samarium and gadolinium oxides were treated at 1100°C, 1200°C and 1400°C, respectively, during 1 hour to obtain the hexagonal or monoclinic phase (high temperature forms). The three as-prepared powders were also treated at 400°C, 800°C and 1000°C, respectively during one week to eventually induce phase reversibility.

Purity of the phases was verified by XRD using a diffractometer PANalytical X'Pert MDP-PRO, Bragg-Brentano geometry, equipped with a Cu $K\alpha_{1,2}$ radiation X-ray. Patterns were collected at 45 kV and 40 mA between 8° and 80° (2θ) with a step size of 0.02° and a time per step of 0.47 second.

The RE_2O_3 structural networks were drawn thanks to Diamond software (Crystal Impact) and imported CIF files from ICSD database (ICSD number are listed Table 1).

3. Results and discussion

3.1 A, B and C crystal structure descriptions

The Fig.3a shows the C-type structure in the classic representation of C-type RE_2O_3 compounds with the space group I a -3. All cations are located in an anionic distorted oxygen octahedral cage. This representation does not allow a clear understanding of the structural framework for further discussion with both their A or B-type filiation. A representation considering a cation close-packed structure, *i.e.* with anions in the centre of the cationic polyhedral cages, makes the crystalline periodicity representation clearer. On Fig.3b, it can be noted that cations form a face centred cubic (FCC) system (with a_{FCC} cell parameter). With this cationic FCC unit scheme, it can clearly be seen the filling of 3/4 of the 8 anionic tetrahedral sites, only. One FCC-like cell (sub-cell), as isolated, constitutes only the 1/8 of the unit-cell (so with a unit cell parameter such as $a = 2\times a_{FCC}$) which is necessary to describe the complete structure of the C-type phase (Fig. 3c), i.e. to describe the periodic organisation of the anionic vacancies. About this anionic vacancy positioning, whatever the RE_2O_3 composition, two first-neighbouring oxygen vacancies sites are always situated along the same FCC-like cell diagonal, *i.e.* in two opposite corner-shared tetrahedral sites. Furthermore, in the unit-cell, for each anionic column associated with four cationic tetrahedral cages, only three are filled with oxygen anions.

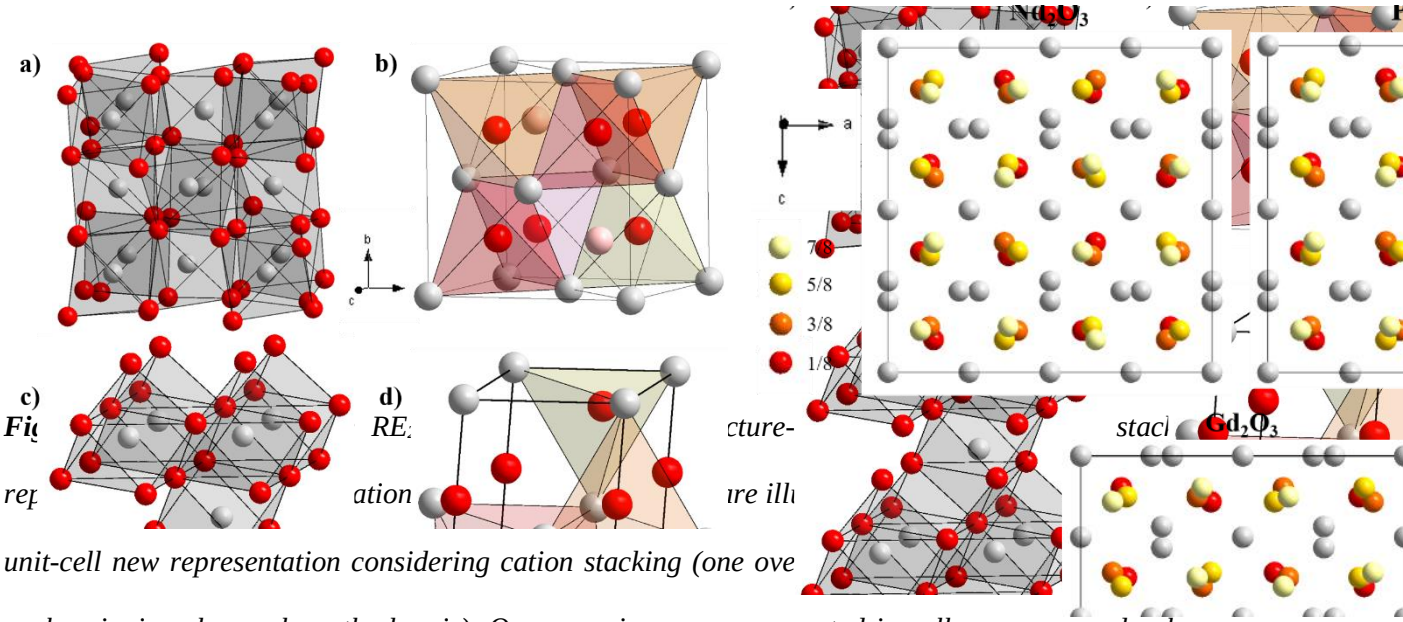

Fig* *RE*₂*O*₃ *cture-* *stac* *rep* *ation* *ıre illu*

unit-cell new representation considering cation stacking (one ove

each anionic column along the b axis). Oxygen anions are represented in yellow-orange-red colour and RE cations are in grey.

In the case of both the hexagonal structure, A (SG: P-3 m 1) and the monoclinic B crystallographic structure B (SG: C 1 2/m 1), the cations are located in a seven-fold coordination environment. The variation of the local distortion of the seven-fold anion cages depending on the RE element explains the occurrence of the two different space groups. As for the C form, the reinterpretation of the two structures, by considering the cationic structural stacking, allows the description of the anionic polyhedra and a clearer view of the periodic framework-type. The A hexagonal cell considering cation stacking is shown in Fig.4a. The B-type system, more complex, is shown in Fig.4b. Similarly to the work performed with the FCC-type cell for the C-type structure, it is possible for the B-form, considering the cation stacking representation, to redraw a unique unit pattern (sub-unit cell) corresponding to a distorted hexagonal unit-cell as evidenced in Fig.4b. Thus, A and B-forms, at the exception of slight angle distortions, both A and B type-structures can be described with this unique unit-pattern hexagonal-like cell (HC-cell). In this HC-like cell (Fig.4a), the oxygen anions are located in one distorted octahedral site and two highly distorted tetrahedral sites. In the first lower half-height (along the standard c-axis), the single cationic octahedral site is filled, while in the second upper half-height of the cell, the two available tetrahedral sites are filled. Consequently, the two cationic tetrahedral cages are with an exotic edge-sharing situation.

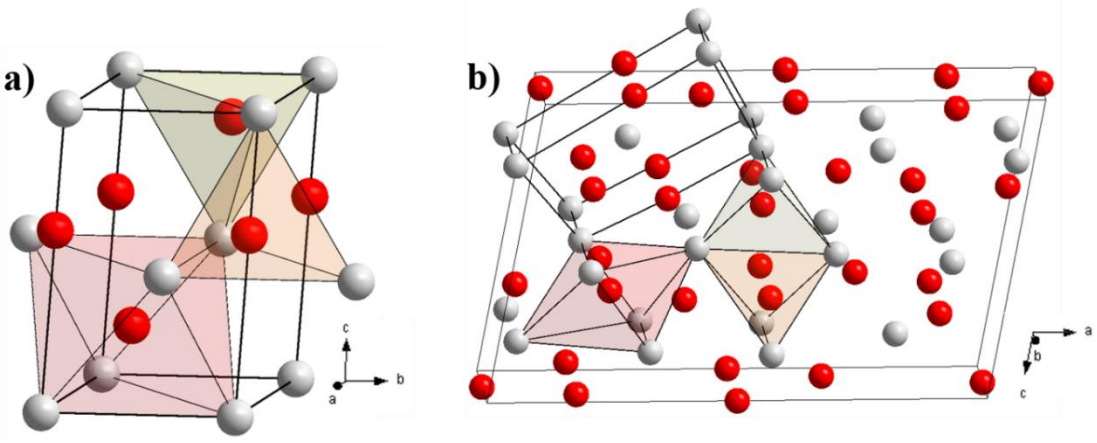

Fig.4 *a) Full unit-cell new representation considering cation stacking for a) the hexagonal A-form and b) the monoclinic B-form. The hexagonal-like cell (HC), allowing the simplification of the B-form representation in a nearly A-cell system, is evidenced on Fig.4b. Oxygen anions are represented in red colour and RE cations in grey.*

On a general point of view, polymorphic transition can be of three types, reconstructive, displacive and dilatational [36]. In the case of RE_2O_3, the cubic to hexagonal or the cubic to monoclinic transitions are reconstructive since changes on the coordination number occur. This reconstructive behaviour is based on the breaking and reforming of anion-cation bonds. To emphasize the structural evolution between C low-temperature form and A or B high-temperature forms, going beyond the new cation stacking representations reported above, the three forms can be represented from the projection along an unique equivalent crystallographic axis (axis perpendicular to the dense cation planes, in our case). Consequently, both the three systems can be plotted as a series of 3 hexagonal-like cells stacked along projection axis (Fig.5). The Fig.5a shows the C-type structure, where the cation atoms deviate from the classical positions by the spreading of the atoms from the 1/3, 2/3, 1/2 axis to the 1/3, 2/3, 1/2 and 2/3, 1/3, 1/2 axes (associated to the ABABAB cation stacking to the ABCABC cation stacking transitions). The Fig.5b show the hexagonal system (A form) clearly respects the standard hexagonal unit cell representation of an inorganic oxide just reversing the anions and the cations. Finally, the reconstruction of the monoclinic type (B form) (Fig.5c) well shows the atomic shift of all anions from their standard positions into a hexagonal system. One can observe the small displacements of the anions located on the c-axis edges of the HC-like cell and the more important displacements of the anions located inside this HC-like cell, while the cations are still roughly located on the standard positions. The similarity between the A and B forms or A and C forms can be clearly distinguished in a glimpse. The transition from the C-type to the A or B-type, consists mainly on a displacement of just few of the cations associated to light local deviations of the surrounding anions. In a way, C to A and C to B phase transitions are both very close the common Blende- to Wurtzite-type phase transformations.

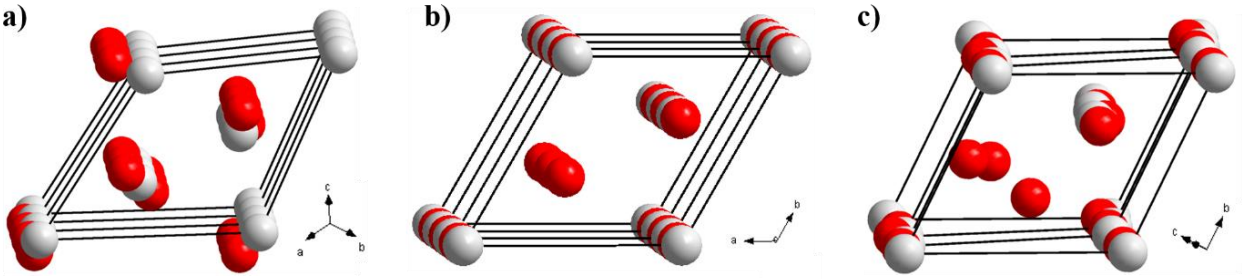

Fig.5 *Representation in a common series of 3 stacked hexagonal like cells (HC) emphasizing the structural filiation between the three studied RE_2O_3 structural types: a) C-type, b) A-type and c) B-type. Oxygen anions are represented in red and RE cations in grey.*

3.2. Determination of the surface and volume energies

The purpose of this part is to calculate the total energy of the phases, considering approximations from both the surface energy and the lattice energy (volume energy). First, to simplify the calculations, only C to A transition will be considered for the RE_2O_3 from Nd to Dy, the B structure being a distorted version of the A structure, as previously demonstrated. Indeed, in our model used for energy calculations, only two kinds of bonds are considered, with only two different energies, whatever the distortion of the anion sites: the one corresponding to oxygen – RE bond where oxygen is located inside an octahedral cation cage, the one corresponding to oxygen – RE bond where oxygen is inside a tetrahedral cation cage. In other words, since the distortions are inducing small modulations of the bond valences, they were neglected. Hence, in a first approximation, the electron flux (assimilated to bond valence, BV) of the chemical bonding around the O^{2-} oxygen anions in 6-fold coordination will be equal to 2/6 (1/3) and the bond valence around the O^{2-} in 4-fold coordination is equal to 2/4 (1/2).

The surface energy is then calculated just as on the number of bonds broken on the cutting plane, which is chosen as the natural (hkl) cleaving plane, *i.e*. the one with the highest atomic density (atoms number per surface unit). For the C-phase, with the (111) plane which is the densest one, the calculation is a bit tricky because the (111) area (named hereafter S_{16}) needed for a robust calculus is constituted by 16 unit parallelogram areas (the ab faces of the HC-like cell, named hereafter S_{HC}). The area (S_{16}) on which is performed the calculation is illustrated on Fig.6a; surface construction has been based starting from a pure cationic surface. To respect the anion/cation stoichiometry of the compound

at the surface, several cation-oxygen bonds just above the cationic cleaving plane have not to be cut for maintaining enough anions to keep the charge neutrality of the surface. The number of cations per S_{16} surface unit is so: 4x1/4+12x1/2+9 = 16. Those same cations could be numbered as 4x1/8+12x1/4+9x1/2 = 8 cations per volume unit. Therefore, here, one has to consider that from the choice to cleave the compound structure basing on a cationic surface, there is a relative enrichment of 8 cations per S_{16} surface-unit. To maintain the RE_2O_3 stoichiometry, 12 anions (3/2*8) just above the cleaving surface have so to be maintained (bonded) to the surface cations. These anions are in two different situations: some of them are with three bonds with three different surface cations, the others are with one single bond with only one surface cation. The anions forming three bonds with the cationic plane are prioritized for further incorporation into the surface because obviously, the energy gain to maintain these is greater than for those bound from a single bond. Finally, it leads to the total number of cut bonds per S_{16} unit (linked to the transparent atoms on Fig.6a) equal to 12x1/2+18 = 24 (i.e. 1.5 bonds per S_{HC} parallelogram unit).

In our energy approximation, it has been considered that the equivalent energy of one bond can be considered as proportional to the electron flux, as used in own previous works to discuss phase transition phenomena [22,23]. All cation-anion bond valences in the C form being equal to ½, the surface energy associated is then 24 × ½ / S_{16} = 12/S_{16} or, taking into account the HC-like unit parralellogram face, as reference, = ¾ /S_{HC}.

For the hexagonal structure A, as well as for the B monoclinic structure, the same method is applied. The close-packed plane, so the realistic cutting plane is the 001, *i.e.* the ABAB stacking plan. Two different cases have to be taken into account, here considering that one side of this cationic cutting plane, the metal-oxygen bonds are belonging to tetrahedral sites, on the other side of the cutting plane, these metal-oxygen bonds belong to octahedral sites (Fig.6b and Fig.6c). The calculation area (S_4) is constituted of 4 parallelogram unit areas (S_{HC}). From the same kind of calculation for maintaining the electroneutrality while creating a cleaving plane that for the C-form, the number of cations per S_4 surface-unit is 4×1/4+4×1/2+1 = 4/S_4 while these same cations were counted as 4×1/8+4×1/4+1×1/2 = 2 per S_4^3 volume-unit. To keep the stoichiometry, 3 anions are still linked to the surface, whatever the "octahedral-site side" or "tetrahedral-site side" is considered. For the "tetrahedral site side"

(Fig.6b), 10 bonds, with BV = ½ are broken per S_4 surface unit, leading to associated surface energy equal to 5 / S_4 or 1.25/S_{HC}. For the "octahedral site side", then, 12 RE-O bonds, with a BV = 1/3, are broken (Fig.6c) by surface creation. The energy associated is the 12×1/3/S_4 or 1/ S_{HC}. As, in first approximation, it could be considered that the two configurations (excluding the "octahedral-site side" or the "tetrahedral-site side" from the compound, i.e. beyond the cleaving surface or outside the crystal) are equiprobable, hereafter, the mean value of the two energy is so considered, *i.e.*, (9/8) /S_{HC}.

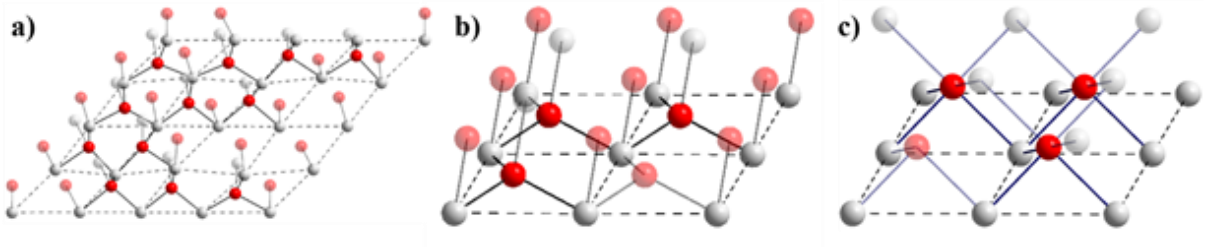

Fig.6 *Representation of the cutting plans of RE_2O_3 forms: a) for the C-type form on the S_{16} surface-unit (16 × S_{HC} parallelograms), b) and c) for the A or B-type forms, on the S_4 surface unit, considering the two configurations: leaving the tetrahedral-site side or the octahedral-site side outside matter. Oxygen anions are represented in red and RE cations in grey, semi-transparent ions (cations or anions) are the ones removed from the surface.*

The volume energy, *i.e.* the lattice energy, is then calculated with same approximation basing on the equivalence between lattice energy and the product of the number of bonds times their bond valence, per volume-unit. In the A hexagonal structure (and equivalently for B monoclinic form), for which calculation is the most simple, the volume unit for the calculation is taken as the hexagonal-like volume unit: V_{HC}, containing 1 octahedral site (6 bonds) and 2 tetrahedral sites (8 bonds). The associated volume energy is so 6×1/3+8×1/2 = 6/V_{HC} (Z=1 / V_{HC}, *i.e.* corresponding to a single RE_2O_3 formula unit). In the C-type form, considering a_{FCC}^3 as calculation unit, containing 6×8 tetrahedra (192 bonds), the associated volume energy is 192 × 1/2 = 96/a_{FCC}^3. a_{FCC}^3 volume unit being associated with Z=16 RE_2O_3 formula units, the calculated energy for an equivalent volume unit that has been performed for A (or B) form is then 96/16 = 6/V_{HC}.

From the calculation, which is performed on the V_{HC} hexagonal-like volume unit, all the polymorphs exhibit same volume energy (same total bond valence flux, in our approximation): $E_r = - K \times 6 / V_{HC}$ (with K a correlating constant in between the total bond flux energy and the real volume energy). Whereas the A or B polymorphs (high temperature forms) exhibit 1.5 times higher surface energy (positive energy) than the C form (low temperature form): E_s (A or B form) = $K \times (9/8) / S_{HC}$ and E_s (C form) = $K\times (¾) / S_{HC}$. Clearly, X-ray diffraction data from the literature reveals (Table 1) that the V_{HC} is subject to a contraction during the low→high temperature transition. Hence, the volume decrease versus the low to high phase transition well supports that the high temperature form gets larger negative volume energy (more stable). It is clear, at this point, that the transition is directly correlated to the surface/volume ratio, *i.e.* is depending to the crystallite size. This could explain the significant disparity of the transition temperatures reported in the literature by the various authors dealing with the subject. Already, the phase transition clearly seems to have to be describe as a phase change materials, with a low temperature phase or kinetic form (stabilized from its low surface energy) and a high temperature form or thermodynamic form (stabilized for the volume energy). Thus, the transition temperatures occur while a critical surface/volume ratio, associated to the phase shift at the total energy crossing point, is reached.

The total phase energy of as-spherical crystallites approximated for all the solid forms can be calculated as:

$E_{tot} = E_r\times V+E_s\times S = E_r\times 4/3\times\pi\times r^3+E_s\times 4\times\pi\times r^2 = -\times 4/3\times\pi\times r^3\times 6\times K/V_{HC} + 4\times\pi\times r^2\times 6/8\times K/S_{HC}$.

It comes that E_{tot}/V is proportional to $-6/V_{HC} + 6/8\times 3/r\times 1/S_{HC}$. For each RE_2O_3 from Nd to Dy, the S_{HC} area unit and V_{HC} volume unit are calculated from the representation on Diamond software drawings using the data of the corresponding CIF files. All the numerical data are provided in Table 1. The $K'\times E_{tot}/V$ curves ($K' = K^{-1}$ as expressed here before) are plotted Fig.7 for each RE_2O_3 in both the cubic (low temperature form in dotted lines) and hexagonal or monoclinic structure (high temperature form in full lines).

Table 1. RE ionic radii, S_{HC} surface area unit and V_{HC} volume unit extracted from the corresponding ICSD files, for all the discussed phases.

RE_2O_3	n°ICSD	Cell type	RE ionic radius (Å) [24, 34, 35]	S_{HC} (Å^2)	V_{HC} (Å^3)
Nd_2O_3	191535	C	0.995	13.3	85.5
	169442	A	1.12	12.7	76.3
Pm_2O_3	647284	C	0.979	13.1	83.0
	647285	A		12.6	75.8
Sm_2O_3	8493	C	0.964	12.9	81.6
	105430	B	1.09	12.5	74.7
Eu_2O_3	431512	C	0.95	12.8	80.2
	659184	B	1.07	12.3	73.4
Gd_2O_3	10173	C	0.938	12.6	18.9
	162248	B	1.06	12.2	72.1
Tb_2O_3	40474	C	0.923	12.5	77.2
	28172	B	1.04	12.0	71.0
Dy_2O_3	248578	C	0.908	12.3	76.0
	160228	B	1.03	11.9	70.1

The curves (Fig. 7) representing the variation of the total energy of both the RE_2O_3 compounds show that low and high temperature forms for each compound intercept at different values of r (particle size), depending on the RE element.

Calculations of energy versus crystallite size are based solely on crystallographic data of room temperature structures. Here, the aim is to show that the transition is well guided by the surface-to-volume ratio of the compounds. In addition, the energies are calculated as proportional to the valence of the bonds, which does not vary with thermal expansion and similarly, the proposed "static" model does not take into account entropic terms. Nonetheless the approximations made, results underline the relevance of this model to explain the irreversible changes between metastable (low temperatures, highly divided powder) and stable (high temperature) forms.

With the increase of r crystallite size, *i.e.* versus the growth of the particles, the surface / volume energy ratio decreases. Because of the less contribution of surfaces with increasing annealing temperature (and so grain size), the high temperature forms become with a lower total energy than the

kinetic ones (low temperature form, with lower surface energy), leading to the transition from C-type towards the A-type and B-type phases. It is clear that a minimal temperature is associated to the transition. But the phase change materials are indirectly associated to temperatures through sintering process or synthesis route because phase transitions are directly tuned through surface/volume ratio. Hence, the thermal treatment rates and duration are also important parameters, which can explain the variability of transition temperatures as-reported in literature.

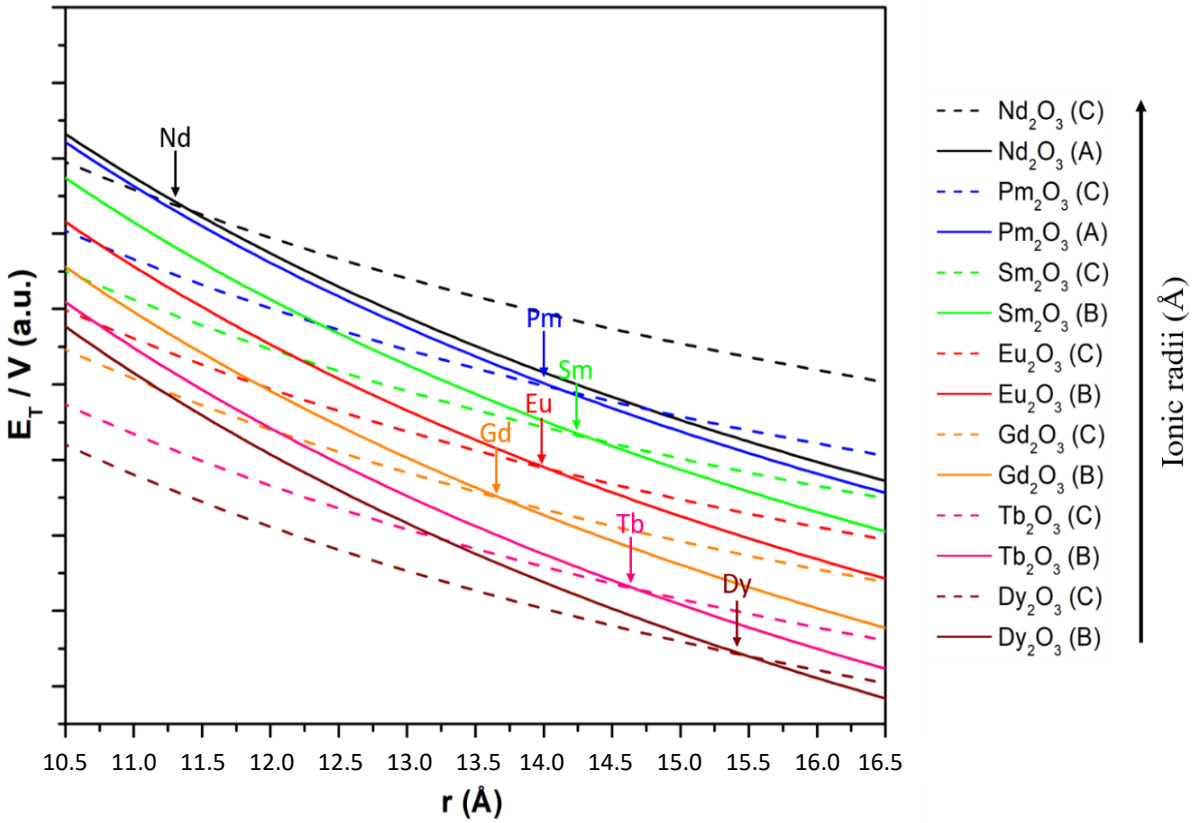

Fig.7 *Plot of the total energy volume as a function of the particle size (r) for high (full lines) and low (dotted lines) temperature forms from Nd_2O_3 to Dy_2O_3 compounds.*

Furthermore, keeping in mind that approximations have been made on s_{HC} unit calculation, especially for the B-type forms, for which the S_{HC} parallelograms are distorted and not perfectly planar, the critical crystallite size for which occurs the phase transition is shown to be dependent of the RE ionic radii. The predicted phase transition temperatures and the crystallite size of the particles both increase with the reduction of the RE cationic radii. The neodymium oxide has the lowest critical crystallite size of the series as well as its reported transition temperature in literature; samarium and europium

compounds present intermediate behaviour while Tb_2O_3 and Dy_2O_3 oxides characteristics belong to the highest proposed values (Fig.2). Considering the just well-established phase change material mechanism for the phase transition, one main aspect governing the irreversible transition is the brutal change of the V_{HC}, with a sharp decrease from low to high temperature form, leading to a densification and so an increase of the volume energy. This decrease of unit-cell volume is associated with, by a reorganisation of the cationic sub-network, a change of some cation positions and cation-anion coordination: from a tetrahedral coordination of the anions in the C-type low temperature form to a mixture of tetrahedral and octahedral anionic coordination in the A or B-type phases. Bigger the cations (longer the cation-anion bond lengths), more pronounced the V_{HC} drop at the transition, shifting so the phase transition from the kinetic (A and B phases) to the thermodynamic phase (C phase) at lower temperatures. This structural reorganization with as stronger amplitude as the RE cation is big, can be correlated to the decrease of the bond covalence/strength, since long ionic bonds exhibit large "elasticity" than short covalent bonds.

Also, it can be noted that the critical crystallite sizes are low (2-4 nm diameter) and not realistic. It can come from the different approximations: (i) the thermal expansion were not taken into consideration calculation being based on V_{HC} and S_{HC} from crystal network assessed at room temperature; (ii) pending bonds formed with atmospheric water are neglected as all surface bonds were considered as cut (over-estimation of surface energies); (iii) surfaces are considered as built only with the densest cationic planes what is not realistic for low crystallite size tending a spherical shapes (under-estimation of the surface energies).

Experimental evidence: introduction

First, a heat treatment of 10 min applied on a mixture of three sesquioxides: Nd_2O_3, Sm_2O_3 and Gd_2O_3, allowed us to determine approximately the transition temperature of these three oxides. XRD patterns were recoreded in 24° - 35° short 2θ range. Respectively, these three oxides change allotropic form at about 900, 1150 and 1250°C. The Nd_2O_3 transition is marked by the appearing of the (101) hexagonal peak concomitant to the disappearance of the (222) cubic form peak (Fig.8a). The Sm_2O_3 transition is marked by the appearing of the (401) monoclinic form peak concomitant to the disappearance of the

(400) cubic form peak (Fig.9a). The Gd_2O_3 transition is marked by the appearing of the (111) monoclinic form peak concomitant to the disappearance of the (222) cubic form peak (Fig.8a).

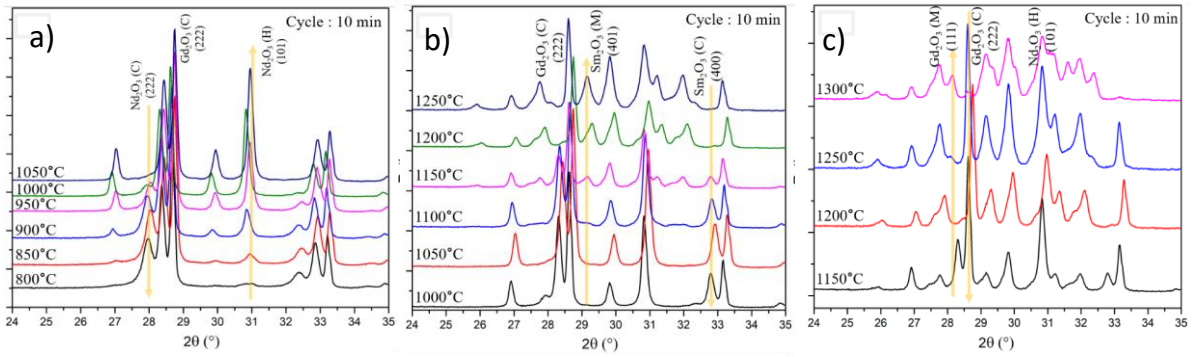

Fig.8 *X-ray diffraction pattern versus thermal treatment temperature of a mixture of the three lanthanide sesquioxides: Nd_2O_3, Sm_2O_3 and Gd_2O_3 showing the low to high polymorph transition of a) Nd_2O_3, b) Sm_2O_3 and c) Gd_2O_3.*

Experimental evidence 1: lack of reversibility

As proof by absurd, an attempt to obtain reversibility by thermal treatment was performed on a series of three lanthanide sesquioxides: Nd_2O_3, Sm_2O_3 and Gd_2O_3 compounds with various transition temperatures. The X-ray diffraction (XRD) patterns of the samples after synthesis and after induction of reversibility from thermal treatment below 400°C about the transition temperatures determined previously (experimental introduction) are reported in Fig.9. For both compositions, hexagonal or monoclinic high-temperature phase were obtained by adequate treatments (above the transition temperature), as described in experimental section. The type-A or B powder is then treated just below the expected phase transition temperature for nano-powder to induce phase reversibility, a dwell time of one week was chosen considering slow kinetics. Whatever the compounds, even after 1 week thermal treatment able to induce reversibility considering a solid-state transition, the high-temperature forms are still the main phase, as-observed on X-ray diffraction patterns. For Sm_2O_3 compound (Fig.9b), after the 1 week post-treatment, a pure monoclinic phase without any trace of cubic peak is observed on X-ray diffraction pattern. Moreover, while besides main monoclinic phase a small fraction of cubic phase is still visible on the XRD pattern for the gadolinium oxide prepared at 1400°C – 1 h treatment, the post-treatment at 1000°C – 1 week, to induce reversibility leads to a pure

monoclinic phase without any more traces of cubic minor phases (Fig.9c). The long treatment duration, at temperature a bit below the phase transformation observed in heating mode, at the opposite of the targeted effect (reversible transformation for high to low temperature form), has induced the full conversion of the cubic phase to the monoclinic one, via the growth of the particle. These two experiments tend to evidence the non-reversible phase change nature of the phase transition. Finally, low intense diffraction peaks associated with cubic phase (low temperature form) are observed on the X-ray diffraction pattern of neodymium oxide retreated for reversibility test at 400°C – 1 week. The presence of cubic phase might be due to remaining amorphous domains or surface hydroxide that crystallized into the cubic phase at 400°C. Indeed, the Nd_2O_3 compound is very hygroscopic and hydroxide formation is difficult to avoid. Those cubic phase peaks present large widths, corresponding to small diffraction domains, estimated using Scherrer equation, at about 30 nm diameter (50 nm for the hexagonal phase). Thus, the presence of the cubic phase cannot be considered as a proof of a beginning of reversibility. More surely, the small cubic phase fraction is issued from the hydroxide minor phases detected initially. Even if can be oppose to our observations that the duration of 1 week of the thermal treatment and/or the chosen temperature do not allow the thermodynamic transformation to occur, these experiments without any doubt, go to the sense, for the three studied compounds, of non-reversible transformation (i.e. in the sense of a mestastability of the low temperature forms).

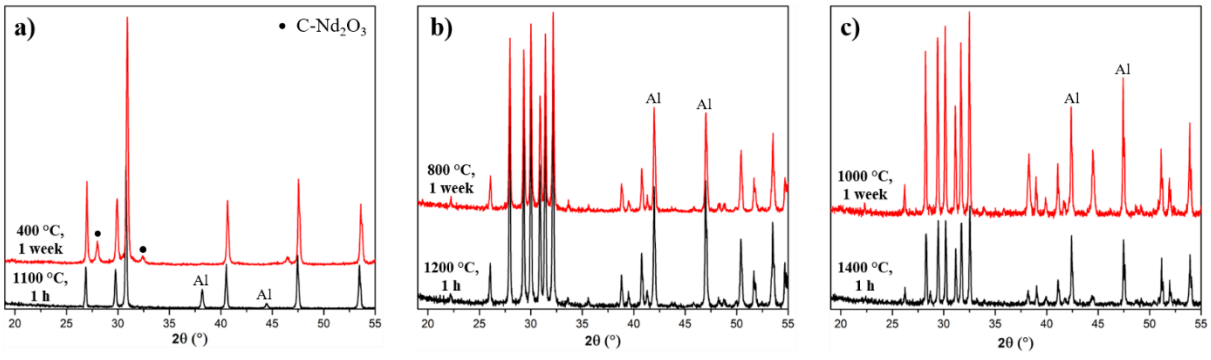

Fig.9 *X-ray diffraction pattern of lanthanide sesquioxides in their high temperature form (after synthesis) and then treated a bit above the phase transformation temperature to induce eventual reversibility, a) Nd_2O_3, b) Sm_2O_3 and c) Gd_2O_3. (Aluminium peaks are due to the sample holder)*

Experimental evidence 2: impact of the crystallite growth of phase change temperature

To demonstrate that the phase transformation is linked to the particle size, two experiments have been performed. First, a pure (cubic phase) neodymium oxide sample and a (cubic phase) neodymium oxide - aluminium oxide mixture were both submitted to 10 min. thermal treatment from 800 °C to 1050 °C, in order to follow the cubic to hexagonal phase transition (Fig.10). The heating rate was 10 K/min; after calcinations, the powders were allowed to cool down slowly to room temperature inside the furnace.

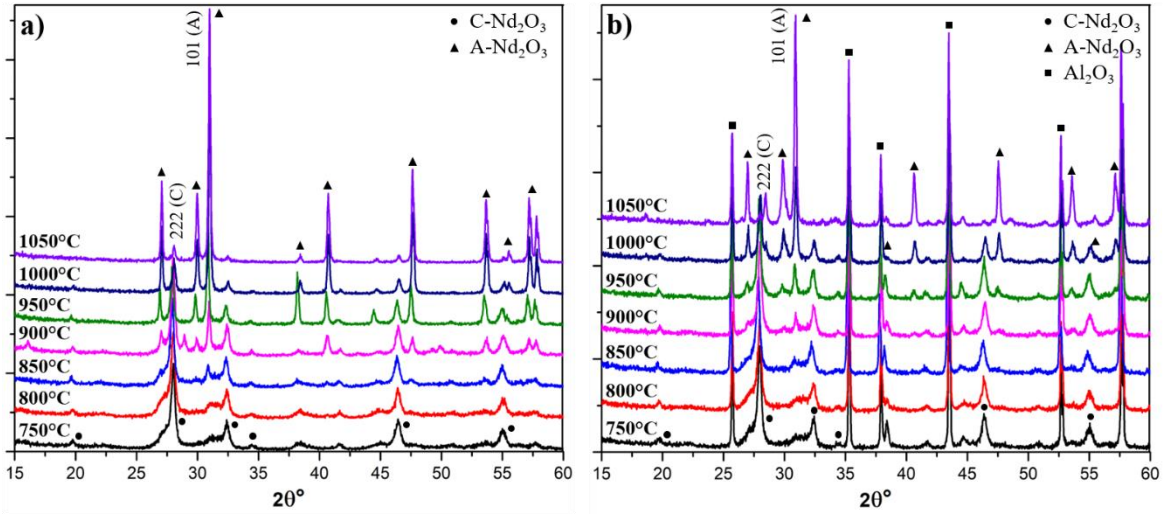

Fig.10 *X-Ray diffraction patterns after thermal treatments at various temperatures of a) a pure Nd_2O_3 sample and b) a 20-80 wt% Nd_2O_3 - Al_2O_3 mixture.*

The large amount of Al_2O_3 was used in the mixture in order to limit the sintering of Nd_2O_3 and thus the growth of its crystallites with the increase of the temperature compared to the pure Nd_2O_3 sample. It can be noted that regardless the heat treatment applied, Al_2O_3 and Nd_2O_3 are the only two phases still observed (in agreement with the preparation of the $NdAlO_3$ ternary oxide, requiring a heat treatment of few hours at 1200°C even after an aggressive grinding consisting of wet ball-milling the Al_2O_3 and Nd_2O_3 mixture for 12 h in a nylon jar using zirconia balls).

The intensity ratio of the two main peaks corresponding to each phases (222 cubic and 101 hexagonal phases) is plotted Fig.11.

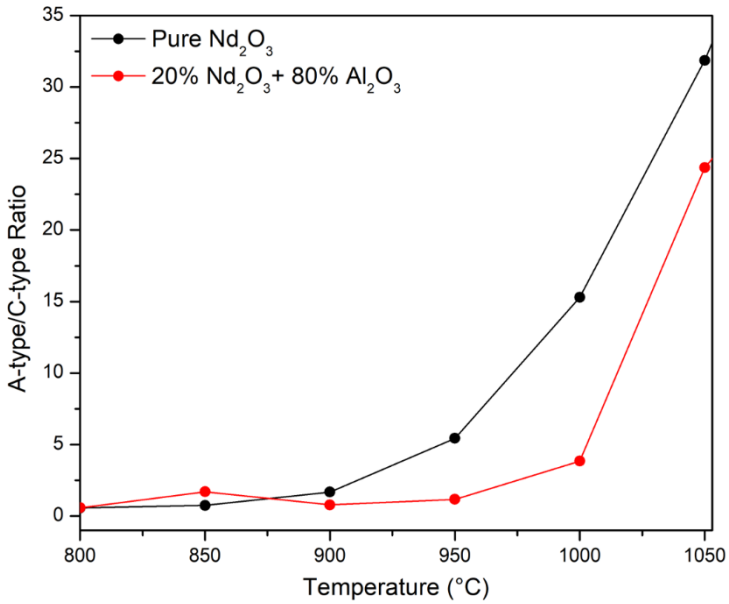

Fig.11 *Plot of the intensity ratio of the main hexagonal peak over the main cubic peak for pure Nd_2O_3 and Nd_2O_3 - Al_2O_3 mixture. The segmented lines are guides for the eye.*

Pure neodymium oxide is subjected to the phase transition around 900°C whereas neodymium oxide mixed with alumina around 1000°C. The transition is significantly delayed, as expected from a non-reversible phase change phenomenon, by the lower growth of the particles due to the diminution of the diffusion paths, due to the presence of alumina grains surrounding the Nd_2O_3 crystallites during the sintering process. Hence, for Nd_2O_3, limiting the grain growth by limiting the sintering effect, is well delaying the phase change from mestatable low temperature form into high temperature form, in heating mode. This shows the correlation between surface/volume ratio and phase change temperature.

Conclusions

The polymorphic transitions between the C cubic form to the A hexagonal or B monoclinic one were deeply discussed through a new approach. The aim is to disentangle the controversy on the classification of Re_2O_3 solid-state phase transition as a reversible solid state phase transition or a non-reversible phase change. First, a clear structure filiation is proposed from Nd_2O_3 to Dy_2O_3 oxides, between polymorphs A, B and C. Second, additional energy considerations based on lattice and surface energy calculations are performed. The lattice volume of all high-temperature forms (for all

RE_2O_3 compounds) is slightly more energetic than the low-temperature forms, with respect to the contraction of the unit cell through the polymorphic transition from low to high temperature. However, the surface energy of the A and B varieties (high temperature forms) is about 1.5 higher than that of the cubic variety (low temperature form). Thus, this phase transition clearly appears as a non-reversible phase change. Also, the transition temperature being correlated to the surface/volume ratio, in addition to the ionic radius RE, the crystallite size appears to be the predominant factor to induce the phase transitions. Our demonstration explains the significant dispersion of phase transition temperatures, which is reported for a single RE_2O_3 compound. Experimental data based on nanopowders of oxides Nd_2O_3, Sm_2O_3 and Gd_2O_3 confirm the non-reversible nature of the phase transition. Moreover, a final examination of the neodymium phase clearly highlights the delay of the temperature transition induced by a lowering of the crystallite size growth.

Conflict of interest

The authors declare no conflict of interest.

Acknowledgements

This study was carried out with financial support of SAFRAN HELICOPTER ENGINES (CNRS collaboration contract n°250374) and the "SATT-Aquitaine Science Transfert" (program: CAPTURES n°2020-163).

References

[1] S.Z.D. Cheng, Chapter 2 - Thermodynamics and Kinetics of Phase Transitions, in: Phase Transitions in Polymers, n.d.

[2] S. Vyazovkin, N. Koga, C. Schick, eds., Handbook of thermal analysis and calorimetry. Volume 6, Recent advances, techniques and applications, Second edition, Elsevier, Amsterdam, Netherlands, 2018.

[3] C. Nobile, P.D. Cozzoli, Synthetic Approaches to Colloidal Nanocrystal Heterostructures Based on Metal and Metal-Oxide Materials, Nanomaterials. 12 (2022) 1729. https://doi.org/10.3390/nano12101729.

[4] G. Gutierrez, E.M. Sundin, P.G. Nalam, V. Zade, R. Romero, A.N. Nair, S. Sreenivasan, D. Das, C. Li, C.V. Ramana, Interfacial Phase Modulation-Induced Structural Distortion, Band Gap Reduction, and Nonlinear Optical Activity in Tin-Incorporated Ga_2O_3, J. Phys. Chem. C. 125 (2021) 20468–20481. https://doi.org/10.1021/acs.jpcc.1c04005.

[5] A.K. Panda, L. Sahoo, R. Chakravarty, N.C. Nayak, R.K. Parida, B.N. Parida, R. Dutta, Transport and semiconducting behavior of Ca_2BiNbO_6 new inorganic double perovskite, Appl. Phys. A. 127 (2021) 950. https://doi.org/10.1007/s00339-021-05105-4.

[6] F. Rullens, N. Deligne, A. Laschewsky, M. Devillers, A facile precursor route to transition metal molybdates using a polyzwitterionic matrix bearing simultaneously charged moieties and complexing groups, J. Mater. Chem. 15 (2005) 1668. https://doi.org/10.1039/b418233b.
[7] S. Wang, K.A. Owusu, L. Mai, Y. Ke, Y. Zhou, P. Hu, S. Magdassi, Y. Long, Vanadium dioxide for energy conservation and energy storage applications: Synthesis and performance improvement, Appl. Energy. 211 (2018) 200–217. https://doi.org/10.1016/j.apenergy.2017.11.039.
[8] M. Li, S. Magdassi, Y. Gao, Y. Long, Hydrothermal Synthesis of VO_2 Polymorphs: Advantages, Challenges and Prospects for the Application of Energy Efficient Smart Windows, Small. 13 (2017) 1701147. https://doi.org/10.1002/smll.201701147.
[9] S. Guan, M. Souquet-Basiège, O. Toulemonde, D. Denux, N. Penin, M. Gaudon, A. Rougier, Toward Room-Temperature Thermochromism of VO_2 by Nb Doping: Magnetic Investigations, Chem. Mater. 31 (2019) 9819–9830. https://doi.org/10.1021/acs.chemmater.9b03906.
[10] S. Guan, A. Rougier, M.R. Suchomel, N. Penin, K. Bodiang, M. Gaudon, Geometric considerations of the monoclinic–rutile structural transition in VO_2, Dalton Trans. 48 (2019) 9260–9265. https://doi.org/10.1039/C9DT01241A.
[11] S. Guan, M. Gaudon, M. Souquet-Basiège, O. Viraphong, N. Penin, A. Rougier, Carbon-reduction as an easy route for the synthesis of VO_2 (M1) and further Al, Ti doping, Dalton Trans. 48 (2019) 3080–3089. https://doi.org/10.1039/C8DT04914A.
[12] G. Salek, A. Devoti, E. Lataste, A. Demourgues, A. Garcia, V. Jubera, M. Gaudon, Optical properties versus temperature of Cr-doped γ- and α-Al_2O_3 : Irreversible thermal sensors application, J. Lumin. 179 (2016) 189–196. https://doi.org/10.1016/j.jlumin.2016.07.004.
[13] G. Salek, A. Devoti, A. Garcia, M. Gaudon, V. Jubera, A. Demourgues, Tuning the composition of rare earth sesquioxides $Gd_{2-x}La_xO_3:Eu^{3+}$ to control phase transitions at a high temperature to design new highly sensitive luminescence-based thermal sensors, RSC Adv. 6 (2016) 55298–55306. https://doi.org/10.1039/C6RA07607F.
[14] V. Blanco-Gutierrez, L. Cornu, A. Demourgues, M. Gaudon, $CoMoO_4$ /$CuMo_{0.9}W_{0.1}O_4$ Mixture as an Efficient Piezochromic Sensor to Detect Temperature/Pressure Shock Parameters, ACS Appl. Mater. Interfaces. 7 (2015) 7112–7117. https://doi.org/10.1021/am508652h.
[15] V. Blanco-Gutierrez, A. Demourgues, O. Toulemonde, A. Wattiaux, O. Nguyen, M. Gaudon, Understanding the Relationships between Structural Features and Optical/Magnetic Properties When Designing $Fe_{1-x}Mg_xMoO_4$ as Piezochromic Compounds, Inorg. Chem. 54 (2015) 2176–2184. https://doi.org/10.1021/ic5025845.
[16] L. Righetti, L. Robertson, A. Largeteau, G. Vignoles, A. Demourgues, M. Gaudon, $Co_{1-x}Mg_xMoO_4$ Compounds for Pressure Indicators, ACS Appl. Mater. Interfaces. 3 (2011) 1319–1324. https://doi.org/10.1021/am2001218.
[17] M. Gaudon, C. Riml, A. Turpain, C. Labrugère, M.H. Delville, Investigation of the Chromic Phase Transition of $CuMo_{0.9}W_{0.1}O_4$ Induced by Surface Protonation, Chem. Mater. 22 (2010) 5905–5911. https://doi.org/10.1021/cm101824d.
[18] M. Gaudon, P. Deniard, A. Demourgues, A.-E. Thiry, C. Carbonera, A. Le Nestour, A. Largeteau, J.-F. Létard, S. Jobic, Unprecedented "One-Finger-Push"-Induced Phase Transition With a Drastic Color Change in an Inorganic Material, Adv. Mater. 19 (2007) 3517–3519. https://doi.org/10.1002/adma.200700905.
[19] S.-C. Zhu, S.-H. Xie, Z.-P. Liu, Nature of Rutile Nuclei in Anatase-to-Rutile Phase Transition, J. Am. Chem. Soc. 137 (2015) 11532–11539. https://doi.org/10.1021/jacs.5b07734.
[20] P.C. Ricci, C.M. Carbonaro, L. Stagi, M. Salis, A. Casu, S. Enzo, F. Delogu, Anatase-to-Rutile Phase Transition in TiO_2 Nanoparticles Irradiated by Visible Light, J. Phys. Chem. C. 117 (2013) 7850–7857. https://doi.org/10.1021/jp312325h.
[21] D.A.H. Hanaor, C.C. Sorrell, Review of the anatase to rutile phase transformation, J Mater Sci. 46 (2011) 855–874. https://doi.org/10.1007/s10853-010-5113-0.
[22] M. Gaudon, Out-of-centre distortions around an octahedrally coordinated Ti^{4+} in $BaTiO_3$, Polyhedron. 88 (2015) 6–10. https://doi.org/10.1016/j.poly.2014.12.004.
[23] I. Trenque, S. Mornet, A. Villesuzanne, M. Gaudon, Discussion on the structural anisotropy of würtzite-type compounds, Solid State Sci. 21 (2013) 81–84. https://doi.org/10.1016/j.solidstatesciences.2013.04.013.

[24] V.M. Goldschmidt, T. Barth, G. Lunde, Geochemical distribution law of the elements. V. Isomorphy and polymorphy of the sesquioxides. The contraction of the" lanthanums" and its consequences, Mat.-Naturv. Klasse. 7 (1925).
[25] A. Iandelli, Sulle modificazioni dei sesquiossidi delle terre rare, Gazzetta Chimica Italiana. 77 (1947) 312.
[26] M.W. Shafer, R. Roy, Rare-Earth Polymorphism and Phase Equilibria in Rare-Earth Oxide-Water Systems, J. Am. Ceram. Soc. 42 (1959) 563–570. https://doi.org/10.1111/j.1151-2916.1959.tb13574.x.
[27] R.S. Roth, S.J. Schneider, Phase Equilibria in Systems Involving the Rare-Earth Oxides. Part I. Polymorphism of the Oxides of the Trivalent Rare-Earth Ions, J. Res. Natl. Bur. Stand. A Phys. Chem., 64 (1960) 309–316. https://do.org/10.6028/jres.064A.030
[28] I. Warshaw, R. Roy, Polymorphism of the rare earth sesquioxydes, J. Phys. Chem. 65 (1961) 2048–2051. https://doi.org/10.1021/j100828a030.
[29] A.G. Boganov, V.S. Rudenko, Stoichiometry and phase transitions in rare earth oxides, Izv Akad Nauk SSSR Neorgan Mater. (1970) 2158–65.
[30] M. Perez y Jorba, F. Queyroux, R. Collongues, Sur une transformation allotropique des oxydes de dysprosium et de gadolinium, bulmi. 84 (1961) 401–402. https://doi.org/10.3406/bulmi.1961.5524.
[31] M. Foex, J.-P. Traverse, Étude du polymorphisme des sesquioxydes de terres rares à haute température, bulmi. 89 (1966) 184–205. https://doi.org/10.3406/bulmi.1966.5951.
[32] M. Zinkevich, Thermodynamics of rare earth sesquioxides, Prog Mater Sci . 52 (2007) 597–647. https://doi.org/10.1016/j.pmatsci.2006.09.002.
[33] B. Wu, M. Zinkevich, F. Aldinger, D. Wen, L. Chen, Ab initio study on structure and phase transition of A- and B-type rare-earth sesquioxides Ln_2O_3 (Ln=La-Lu, Y, and Sc) based on density function theory, J. Solid State Chem. 180 (2007) 3280–3287. https:// 10.1016/j.jssc.2007.09.022
[34] Y. Zhang, I.-H. Jung, Critical evaluation of thermodynamic properties of rare earth sesquioxides (RE = La, Ce, Pr, Nd, Pm, Sm, Eu, Gd, Tb, Dy, Ho, Er, Tm, Yb, Lu, Sc and Y), Calphad. 58 (2017) 169–203. https://doi.org/10.1016/j.calphad.2017.07.001.
[35] R.J.M. Konings, O. Beneš, A. Kovács, D. Manara, D. Sedmidubský, L. Gorokhov, V.S. Iorish, V. Yungman, E. Shenyavskaya, E. Osina, The Thermodynamic Properties of the *f* -Elements and their Compounds. Part 2. The Lanthanide and Actinide Oxides, J Phys Chem. 43 (2014) 013101. https://doi.org/10.1063/1.4825256.
[36] S. Stecura, U.S.B. of Mines, Crystallographic Modifications and Phase Transformation Rates of Five Rare-earth Sesquioxides: Lanthanum Oxide, Neodymium Oxide, Samarium Oxide, Europium Oxide, and Gadolinium Oxide, U.S. Department of the Interior, Bureau of Mines, 1965. https://books.google.fr/books?id=nbr0YBk1sggC.
[37] H.R. Hoekstra, Phase Relationships in the Rare Earth Sesquioxides at High Pressure, Inorg. Chem. 5 (1966) 754–757. https://doi.org/10.1021/ic50039a013.